

Bond behavior between CFRP strips and calcarenite stone

M. Accardi, C. Cucchiara, L. La Mendola

Dipartimento di Ingegneria Strutturale e Geotecnica, Università di Palermo, Italy

ABSTRACT: In this paper a local bi-linear shear stress-slip law with softening is proposed on the basis of an experimental investigation which reproduces the interface calcarenite-CFRP behavior according to several codes. The parameters were calibrated on the experimental results relative to double shear pull tests from which the maximum transferable load in the joint and the strain profiles were obtained. A numerical investigation was carried out by a finite element software including an interface element modeling interlaminar failure and crack initiation and propagation, in order to validate the calibration of the parameters defining this interface law and the accuracy of the recorded measurements.

1 INTRODUCTION

Fiber composite materials are frequently used to strengthen to flexure and/or shear of reinforced concrete structures. The use of composite material has recently been extended to the masonry structures of important historical buildings. The use of composite materials in reinforcing techniques presents particular advantages which include high strength, lightness, resistance to corrosion, ease of application and the possibility of removal.

The effectiveness of this technique is particularly linked to the bond phenomenon that guarantees the maximum transferable load by an adequate transfer length.

Bond behavior between Fiber Reinforced Polymer (FRP) and masonry can be placed in the wider context of bonding of FRP to quasi-brittle materials like concrete, mortar and rock. While extensive research has been conducted and reported in the literature for reinforced and prestressed concrete structures, much less has been reported for masonry structures. Many researchers have studied the characteristics of bonding between the reinforcement system (FRP or steel plates) and the basic materials (usually concrete with different mechanical properties), achieving a good understanding of the related mechanism (Holzenkämpfer (1994); Chajes et al. (1996); Bizindavyi & Neale (1997, 1999); Täljsten (1997); Neubauer & Rostasy (1997); Yuan & Wu (1999); Yuan et al. (2001). The observed modes of debonding for structural elements strengthened with FRP can generally be classified into two types: (a) those associated with high shear and normal stresses near the bonded

plate ends, of which a review of the experimental and analytical approaches can be found in Smith & Teng (2001); and (b) those mainly associated with high bond stresses induced by a discontinuity or pre-existent crack away from the plate ends, of which a review of the experimental and analytical approaches can be found in Chen & Teng (2001). These well-known failure mechanisms for RC structures are also common for masonry structural elements and they have been classified according to Italian Recommendations CNR DT 200-2004 as *plate end debonding* and *intermediate crack debonding* respectively.

Some codes and recommendations have been introduced in the last few years, in order to regulate the use of FRP for strengthening existing structures. Among the experimental tests which have been performed for bond evaluation (double or single shear pulling test, double or single shear pushing test, beam test), the double pull test has been the most usual test method proposed by the standard codes (JSCE 2001). Two plates or strips are bonded on opposite sides of a concrete block and equal tensile forces F are applied to the plates. These forces are balanced by a pulling force applied in the basic material $2F$ which may be applied either through a steel bar embedded in the centre of the concrete block, or through steel plates bonded to the sides of the basic material. The double pull test may not divide the shear force symmetrically on two sides of the specimen. For this reason it is appropriate to use the same measurement for each side in order to verify correct division of the force. Following an extensive literature review it appeared that test specimens usu-

ally failed at few millimeters into basic material below the adhesive. The most relevant output of a bond test, beside the bond strength of the specimen, is the measured relationship between the bond stresses (that is the shear stress along the length of the reinforcement as a response to the external load) and the slip (defined as the relative displacement between the reinforcement and the basic material). Considerations on the local bond stress slip relationship will be presented in this paper. It is worth noting that different local bond-slip curves for FRP-to-concrete bonded joints have been proposed (Nakaba et al. 2001; Savoia et al. 2003; Leung 2004; De Lorenzis et al. 2001).

On the basis of an experimental investigation carried out by the authors in a previous study, an understanding of the interface adherence characteristics is carried out in the present paper, referring to the reinforcing technique of using the wet-lay-up method applied to structural masonry elements consisting of calcarenite stone and bed joint mortar. In particular the focus of this paper is to propose a local stress-slip law calibrated on the experimental results which reproduces the interface behavior between calcarenite and Carbon Fiber Reinforced Polymer (CFRP). The bond stress-slip curves obtained by experimental results can be modelled by a bi-linear law with linear softening, as proposed in several codes. This statement is validated by a numerical analysis based on a finite element method in which an interface element is utilized of which the parameters are maximum bond stress, relative slip and fracture energy.

2 MATERIALS

The study of the bond behavior between FRP and masonry material providing support, requires the physical and mechanical properties of the structural materials involved. The mechanical propriety of calcarenite stone (the resistant element of masonry material) and FRP, determined by standard tests, will be introduced here for this purpose.

2.1 *Calcarenite stone*

Organogenic calcarenite is a structural stone widely used for historical buildings of architectural interest in the Mediterranean area. It is generally recovered in blocks and is located in a wide and elongated area approximately parallel to the shore line. It has marked heterogeneity and high total open porosity and the colour can change from greyish white to dark red.

The calcarenite stone used in the experimental investigations to which this paper refers, were recovered from a quarry located in western Sicily. The ashlar of this calcarenite stone have average dimen-

sions of 210x160x360 mm. The cubic and prismatic specimens used to determine the mechanical properties were recovered from the same ashlar to make up the pull test specimens as shown in Figure 1.

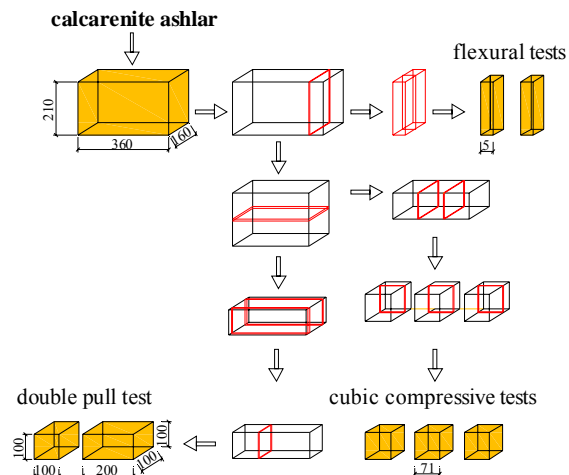


Figure 1. Specimens for mechanical properties and adherence characteristics.

Compressive cubic tests were carried out by a universal testing machine operating in displacement controlled mode with maximum capacity equal to 600 kN. Results are utilized to obtain a correlation between the fracture energy of each pull-out test and the relative cubic compressive strength of the calcarenite ashlar; this correlation is proposed in the following sections.

2.2 *CFRP reinforcement*

The composite material used here as externally bonded reinforcement consists of two combined materials: high-strength fibers and matrix. The fiber provides the strength of the composite, and the matrix is the product that holds the fibers together and acts as a load transfer medium. The fiber used in the experimental program is a unidirectional carbon fiber fabric, of which the mechanical characteristics, as indicated by the manufacturer, are the following: tensile strength 3450 MPa; elongation break 1.5% and tensile modulus 230000 MPa. The epoxy resin used in this experimental program is a two-component, 100% solid, non-sag paste and light grey in colour. The mechanical properties of the epoxy resin provided by the manufacturer are the following: tensile strength 30 MPa; elongation break 1.5%; flexural modulus 3800 MPa.

Use of the CFRP system to strengthen structural masonry elements introduces new properties which it is essential to know, starting from the physical and chemical characterization of the interphase CFRP-masonry substrate. The interphase characterization was carried out through microscopic imaging analysis from which it is possible to observe that FRP application on the surface creates a new layer, usually called the interphase, where the matrix used to bond

the reinforcement soaks the substrate material (see Fig. 2).



Figure 2. Optical microscopy observation of calcarenite-CFRP interface.

A better understanding of the behavior of this crucial zone, where molecules of the two materials interact creating properties that differ from those of the two separate phases, is vital to improve the way in which materials are combined together.

3 EXPERIMENTAL INVESTIGATION

A synthesis of previous experimental research carried out by the authors is presented in the following paragraphs; details can be found in Accardi & La Mendola 2004.

3.1 Specimen

Double Shear pulling Tests (DST) were carried out with the purpose of determining the pull-out load and the effective transfer length. Specimens consisted of two calcarenite blocks loaded through steel bars previously inserted into them and sealed with epoxy resin (see Fig. 3). In particular the prismatic block was that in which the bond phenomenon was evaluated while the cubic part was the anchorage. The latter was made by wrapping the faces of the cube with the same CFRP strips as used for the bond test. Specimens were prepared with three different bonded length: 50, 100 and 150 mm. The external load yielded two shear forces in the CFRP strips bonded onto each side of the strengthened block.

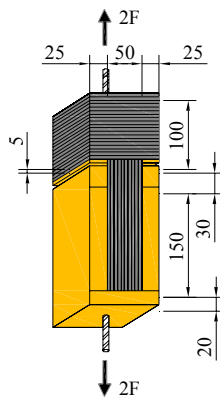


Figure 3. Specimen for pull-out test with bond length 150 mm.

Using this scheme, nine specimens were prepared for each bond length; the same width of CFRP strip was used ($b_f = 50$ mm), as the tests were intended to estimate the effective bond length, i.e. the length be-

yond which any increase in bond length cannot significantly increase the maximum transferable load.

3.2 Loading and measurement

Each specimen was set in a displacement controlled universal testing machine with maximum capacity equal to 600 kN and subjected to pure tensile force through steel rods causing direct shear on the CFRP strips. Spherical joints were placed at the top and bottom grips to avoid any bending moment caused by eccentricity. For some specimen, in addition to the maximum load-carrying capacity, the total displacement at the section in which the tensile force was applied for each side was measured at each load step by using two LVDTs. Moreover, electrical strain gauges on both of the opposite reinforced sides were fixed along the centre line of the CFRP strip to assess the variation in normal stress along the length of the reinforcement and the bond stress variation at the CFRP-calcarenite interface. Data from load cell, LVDTs and electrical strain gauges were recorded by a data acquisition system. The measurement system of the displacement at the section in which the tensile force was applied and the location of the gauges on one side are shown in Figure 4.

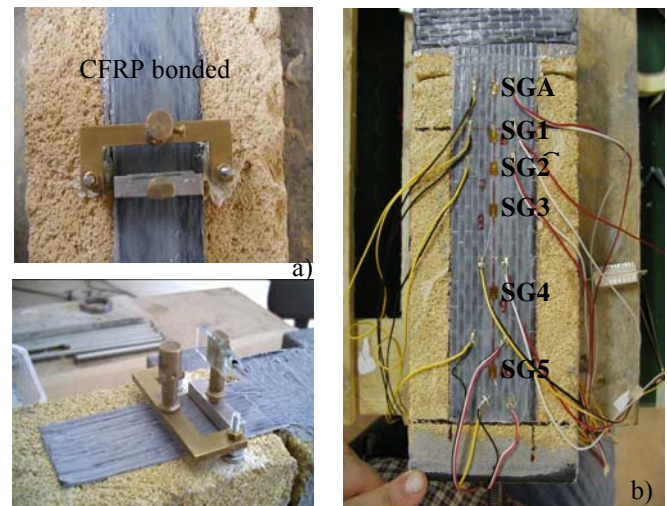


Figure 4. Measurement devices to record a) slip at the loaded end; b) strain profiles along the bonded length.

The local measurement system allows the definition of the effective part of the bonded length where the stresses are applied on the reinforcement transfer within the basic material, with a degree of accuracy related to the gauge spacing.

Since the stress gradient in the regions near the strip end is high, the gauge spacing was made smaller to ensure greater accuracy in computing the CFRP axial strains and the transfer length.

3.3 Results

All specimens were subjected to tensile force until total bond failure took place. Typical failure started

and developed inside the calcarenite block until total debonding of the reinforcement occurred. The thickness torn off the calcarenite block was estimated to be approximately 1.5–2.0 mm, depending on the epoxy resin penetration capability (see Fig. 2). Results of the tests in terms of maximum external load recorded (pull-out load F_u) and corresponding cubic compressive strength are contained in detail in Accardi & La Mendola (2004).

Results in terms of the curves *pull-out load (F) - displacement at the loaded end (U)* of all tests showed similar initial linear elastic behavior with stiffness. $\bar{K} \approx 75000 - 90000 \text{ N/mm}$

Tests with L=100 and 150 mm bond lengths revealed similar behavior characterized by a constant load increase until the first cracking at the loaded end occurred; this was followed by progressive debonding process up to failure. By contrast, tests with L=50 mm revealed a lower pull-out load accompanied by very brittle failure, making measurements impossible; these tests did not show any cracking process and the failure mode was quite different than that for specimens with L=100 and 150 mm.

In Figure 5 strain profiles recorded by strain gauges are reported for two specimens with bond length 100 and 150 mm. Each strain profile is plotted for a given load level. The trend of the strain distribution is in agreement with that recorded by experimental tests carried out on concrete (Bizindavyi & Neale 1999). In the elastic range the strain distribution for both tests follows an exponential decay law from the loaded end to a length between 40 and 80 mm. The elastic limit is about 0.75–0.85 times the maximum load. When the load increases the curves change shape until their concavity changes.

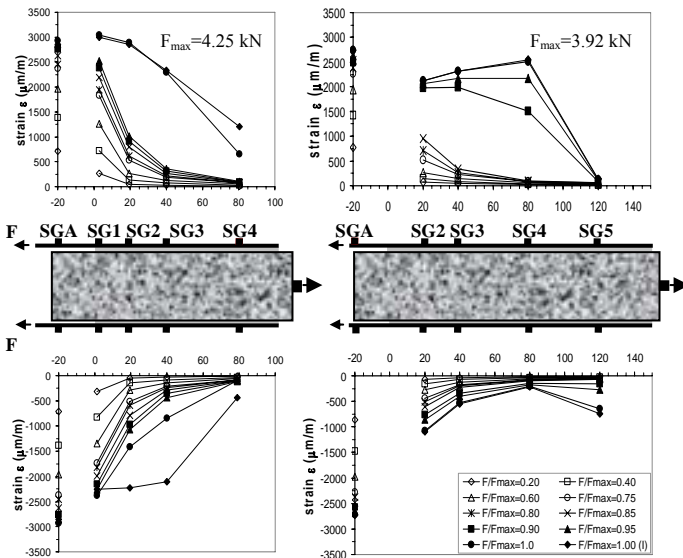


Figure 5. Strain profiles along the length of CFRP strip: (a) L=100mm and (b) L=150mm.

When total debonding starts, the values of two consecutive strain gauges become almost equal.

The analysis of the recorded data allows the identification of two bond lengths: - in the elastic range the strain profile reaches negligible values between the gauges located at 40 mm and 80 mm; this distance defines the so-called initial transfer length l_b in which the joint is characterized by elastic behavior; - when the load increases the gauges located at 80 mm begin to measure significant strain values; then the effective bond length L_b is identified as the distance between the loaded end and the ultimate point where the strains are not negligible; this measurement was made when the strain value of the first gauge in the bonded length was almost equal to that measured outside.

The effective bond length is evidently longer than the minimum transfer length l_b . After this stage, the load is almost constant but the debonding increases, shifting the effective bond length until the CFRP strip has completely peeled from the matrix. It can be observed that the results presented above lead to the fact that $80 \text{ mm} < L_b < 120 \text{ mm}$ and that the L_b shifting is more evident for the specimen with L=150 mm. The debonding propagation process is completely absent in the specimens with L=50 mm; for this reason the strain profiles are not discussed here.

From the strain profiles measured along the CFRP length it is possible to trace an experimental local bond stress-slip curve in the distance between two strain gauges in accordance with Savoia et al. (2003).

By considering an elastic behavior of the CFRP strip, the average value of the bond stress between two subsequent strain gauges ($i, i+1$) can be written as a function of the difference of the measured strains as:

$$\tau_{i,av} = \frac{A_f \cdot E_f (\varepsilon_{i+1} - \varepsilon_i)}{b_f (x_{i+1} - x_i)} \quad (1)$$

where A_f , b_f and E_f are the cross-section area, the width and the elastic modulus of the carbon fibers respectively. Moreover, by assuming that complete compatibility occurs at the first strain gauge position (no slip) and the calcarenite strain is negligible with respect to the CFRP, integration of the strain profiles gives the following expression for the slip at distance \bar{x} from x_i , with $0 \leq \bar{x} \leq (x_{i+1} - x_i)$:

$$s(\bar{x}) = s(x_i) + \int_0^{\bar{x}} \varepsilon(\bar{x}) d\bar{x} = s(x_i) + \frac{(\varepsilon_{i+1} - \varepsilon_i) \bar{x}^2}{(x_{i+1} - x_i) 2} + \varepsilon_i \bar{x} \quad (2)$$

Taking \bar{x} as the average value of the strain gauge spacing $\bar{x} = (x_{i+1} - x_i) / 2$, Equation (2) yields:

$$s(\bar{x}) = s(x_i) + \frac{1}{2} (x_{i+1} - x_i) \cdot \left[\frac{(\varepsilon_{i+1} - \varepsilon_i)}{4} + \varepsilon_i \right] \quad (3)$$

The average value $s(\bar{x})$ of slip between x_i and x_{i+1} is then computed. For all segments between two

consecutive strain gauges locations, couple of values $(\bar{\tau}_{i,av}, s(\bar{x}))$ can be obtained. Results obtained in this way show similar behavior characterized by an elastic ascending branch with slope within $k=70\text{--}120\text{ N/mm}^3$ up to bond strength and afterwards a descending branch. In Figure 6, for two tests with $L=150\text{ mm}$ and two tests with $L=100\text{ mm}$ the bond stress-slip curves are given for the segment between SG2-SG3.

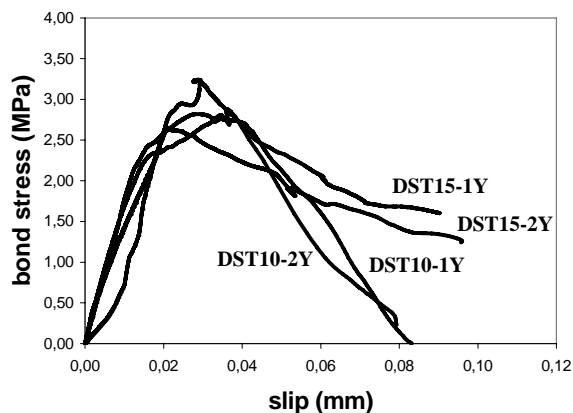


Figure 6. Local bond stress-slip law for specimens with different bonded length.

Tests with bond length $L=150\text{ mm}$ exhibit in the softening branch a gradual stress reduction with further sliding. This is probably correlated to the friction present between the two surfaces. Tests with bond length $L=100\text{ mm}$ show the same trend as each other but with a different slope in the softening branch if compared with the 150 mm bond length specimens. It is worth noting the absence of the sub-horizontal branch probably because of the shorter length adopted in this test.

These findings were also in the experimental analysis carried out for concrete specimens strengthened with steel plates and reported in Holzenkämpfer (1994).

4 DEBONDING MECHANISM

The available analytical models are basically addressed to evaluating the elastic stiffness (service condition) and bond strength (ultimate condition), using often different approaches for the same problem: *stress approach*, in which the criterion for growth of the debonded FRP-matrix interface is expressed in terms of the interfacial bond stresses; and the *fracture mechanics approach*, in which the criterion for interfacial debonding is expressed in terms of energy balance (Accardi & La Mendola 2004). But the elastic stiffness, as well as the energy that is available for crack growth and the debonding process, need to be clarified. To gain a clear understanding of load transfer mechanism and crack propagation along the CFRP-calcarenite interface, numerical analyses were carried out to simulate the behavior of

the Double Shear pulling Test, based on the LUSAS finite-element program using an appropriate interface element that support a damage model (Qiu et al. 2001).

4.1 Analysis of bonded joint in linear elastic range

The analysis of the bonded joint in the linear elastic range can be carried out by means of a simple shear lag approach.

Täljsten (1996), Wu et al. (2002) suppose uniformly distributed axial stresses in the cross-section of the matrix, neglecting the fact that the bond phenomenon develops around a thin layer near the reinforcement. By contrast, De Lorenzis et al. (2001) suppose rigid block basic material and attribute deformability only to the adhesive and/or primer layer. However, by using F.E.M. in a linear elastic analysis, it is possible to see that the load transfer mechanism is concentrated in a layer near the reinforcement. Usually this layer also involves the basic material. According to the CNR DT 200-2004 Recommendation, it is therefore possible to take a basic material layer into account to define the elastic deformability.

By introducing the values of E_c and ν_c for calcarenite stone given in Arces et al. (1998) we obtain:

$$G_c = \frac{E_c}{2(1+\nu_c)} = \frac{9000}{2(1+0.2)} = 3750\text{MPa} \quad (4)$$

Assuming the following expression for the slope of bond stress-slip curve:

$$k = \frac{G_c}{t_c} \quad (5)$$

and by using the experimental values above obtained it is possible to deduce the thickness $t_c=31.25\text{--}53.57\text{ mm}$ involved in the elastic deformability. The t_c values are in agreement with the elastic FEM analysis, as shown in Figure 7.

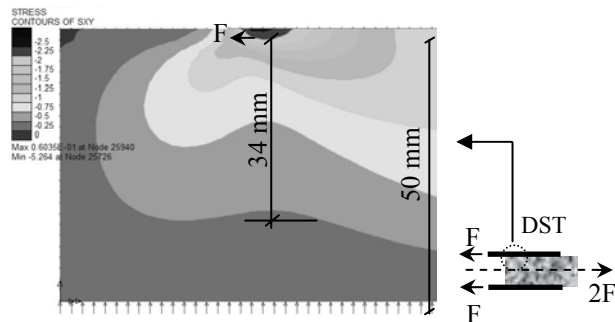


Figure 7. Shear stress contours of DST close to loaded end.

4.2 Progressive debonding process

The connections between the reinforcement and the basic material were modelled by the discrete element in the LUSAS program named IPN6 that in a 2D configuration is an interface element between two lines with quadratic interpolation. This type of

element inserted at the lines of potential debonding proves to be particularly suitable for modelling inter-laminar failure and crack initiation and propagation. The element has six nodes and no thickness, describing the relationship between the stresses and relative displacements of the nodes connecting the two faces.

These interface elements support a damage model named *Delamination Damage Model* (see Figure 8) characterized by the failure modes, *Opening* and *Sliding*. In the following sections the uncoupled delamination option mode will be chosen in order to avoid the mode I failure. This model reproduces the nonlinear response of a system with potential debonding planes.

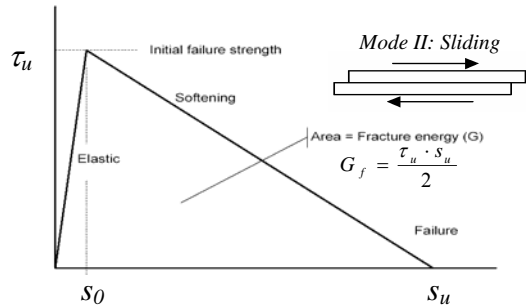


Figure 8. Reinforcement of basic material connection: bi-linear with linear softening interface law and sliding fracture mode.

The behavior follows a linear law up to the strength threshold value τ_u (initial failure strength), which corresponds to the limit displacement s_0 . When this value is exceeded, linear softening behavior occurs up to the point at which the fracture energy G_f is dissipated. Complete separation occurs when the maximum relative displacement (s_u) is reached. Therefore this damage model is capable of describing the mode II failure (sliding) associated with shear interface stresses. Hence the failure mode requires three parameters to describe the interfacial behavior: failure strength (τ_u), corresponding slip (s_0), and fracture energy (G_f).

The τ_u and s_0 parameters can be determined from the experimental values of each bond test and reported in Table 1 with the maximum load F_u and the fracture energy G_f . The latter is evaluated by using the expression of maximum load F_u obtained from Holzenkämpfer (1994) and Täljsten (1996) by using the fracture mechanics approach considering a Mode II (shear) fracture mechanics of the basic material:

$$F_u = b_f \sqrt{2E_f t_f G_f} \quad (6)$$

in which t_f is the thickness of CFRP and the other symbols as defined above

Data for G_f given in Table 1 are obtained from Equation (6), in explicit form:

$$G_f = \frac{F_u^2}{2b_f^2 E_f t_f} \quad (7)$$

by introducing the following values: $b_f = 50$ mm, $t_f = 0.13$ mm, $E_f = 230000$ N/mm².

Table 1. Bond properties for DST (numerical parameters)

Specimen code	F_u [N]	s_0 [mm]	τ_u [MPa]	G_f [N/mm]
DST15-1Y	5040	0.053	3.76	0.168
DST15-2Y	3920	0.032	3.82	0.103
DST10-1Y	4930	0.038	4.39	0.163
DST10-2Y	4250	0.050	3.50	0.116

Using the values identified for each specimen, the comparison in terms of F - U curves is reported in Figures 9 and 10 for the bond tests with bonded length 100 and 150 mm respectively.

The numerical-experimental comparison identifies three different phases: elastic behavior, debonding propagation and snap-back branch; the latter numerically assumed only because it is very difficult to point out experimentally. The numerical model is able to describe the elastic stiffness and to predict the maximum pull-out load because the latter is related to the fracture energy only (Yuan et al. 2001).

It is worth noting that the pull-out load and stability of the debonding propagation are influenced by the asperity interlock, the roughness and the shape of the debonded surface.

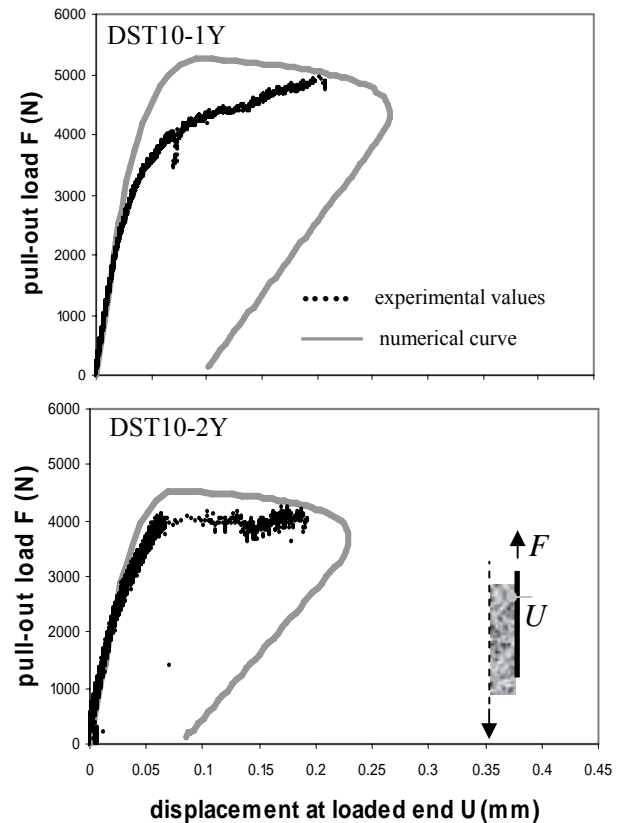


Figure 9 Comparison between pull-out load vs. displacement curves with $L=100$ mm bonded length.

These aspects determine a different friction between the reinforcement and the debonded surface that could modify the debonding behavior of the

specimens as shown in the experimental curves reported in Figures 9 and 10. The friction is more evident for granular material like the calcarenite stone used in the present experimental investigation, whose specimens appear to be mostly made up of small grains joined by calcite with low bond strength.

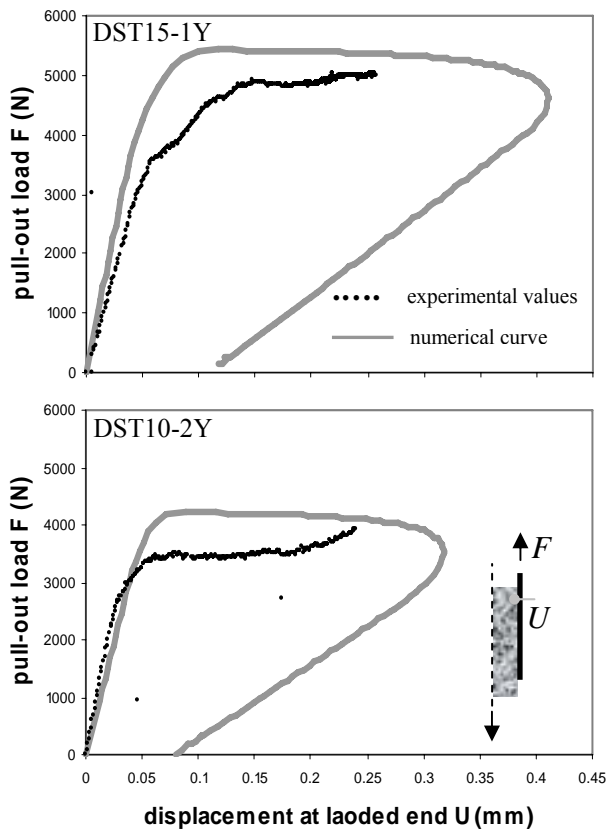


Figure 10. Comparison between pull-out load vs. displacement curves with $L=150$ mm bonded length.

4.3 Experimental correlation for debonding limit strain

The results obtained allow the deduction of an important parameter, the fracture energy G_f , which is defined as the energy required to take the area of a bonded surface to complete fracture. It is worth noting that the descending branch of the bond stress-slip curve has a major influence on the fracture energy.

Equation (7) correlates the bond strength of the joint with the fracture energy. However, the failure mode starts and develops within the calcarenite stone, thus the fracture energy depends mainly on the mechanical properties of the base material.

Recently, some studies have been carried out on a procedure to measure the critical mode II strain energy release rate and to identify the fracture energy G_f . In present-day applications identification of the fracture energy is very difficult, especially for existing structural elements. For this reason, the existing design models for concrete (ACI 440-2000; JSCE 2001; fib 2001; CNR-DT 200-2004) and masonry

(CNR DT 200-2004) correlate G_f with the mechanical properties of the basic material, as compressive and tensile strengths. Hence, by referring to Equation (7) and by introducing the F_u values obtained by the experimental tests it is possible to find out an experimental correlation between the compressive strength of calcarenite stone used to make up the specimens in the pull tests and the fracture energy. Specifically, the data of the DST with bonded length 150 mm were recorded. The specimens with $L = 150$ mm have a higher bonded length than the effective transfer length, as pointed out earlier. The values used in Figure 11 are given in Accardi & La Mendola (2004) and Failla et al. (2002).

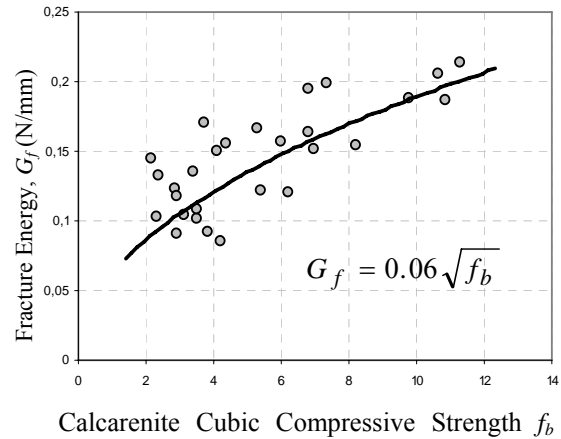


Figure 11. G_f - f_b experimental correlation.

The choice of cubic compressive strength as a mechanical parameter of the basic material to correlate with the bond strength instead of tensile or shear strength is due to the use of simple and reliable experimental tests, particularly for an anisotropic material like calcarenite stone.

Substituting the correlation indicated in Figure 11 in Equation (6) it therefore yields the following equation:

$$F_u = b_f \sqrt{0.12 E_f t_f \sqrt{f_b}} \quad (8)$$

which gives the bond strength of the CFRP-calcarenite joint.

Chajes et al. (1996) have already proposed a correlation between the ultimate pull-out load F_u of the FRP-to-concrete bonded joint and the $\sqrt[4]{f_b}$ but only in Chen & Teng (2001) has this been confirmed through an extensive review of available experimental data.

The experimental correlation obtained for Sicilian calcarenite base material shows a possible extension of predictive bond strength models to natural stone treated like concrete with low compressive strength. Nevertheless, the lack of experimental results on various natural stones does not make it possible to generalize the method proposed here. However, it should be noted that the correlation presented here could also be valid for a soft rock like Naples tufa (Cosenza et al. 2000) but is not applicable to harder

stone like Leccese stone (Aiello & Sciolti 2004), which instead shows less bond strength than the expected values. The failure mode is also different; for Leccese stone the FRP only involves a very thin layer of stone attached to the composite strip, and this is probably due to the different grain size and porosity of the rocks. For this reason it could be useful to introduce other parameters of the basic material that regard the porosity, the grain size or the structure of the rock.

5 CONCLUSIONS

The experimental and numerical investigations highlighted the behavior of the CFRP-calcarene bonded joint. The use of external strain gauges placed along the CFRP bond length made it possible to record strain profiles and to deduce a local bond stress-slip law for the CFRP-calcarene interface.

The numerical model does not show significant differences to predict of the maximum pull-out load and to describe the experimental behavior of the DST specimens. Nevertheless it is worth noting that the experimental measurements recorded for specimens with bond length $L=100$ mm and $L=150$ showed a different slope in the softening branch that reveal the presence of friction between the two debonded surfaces that could modify the post-peak branch of the local bond-slip law.

It is therefore necessary to consider the role of friction in order to better describe the specimen behavior for different experimental setups and other experimental tests .

REFERENCES

Accardi, M., La Mendola, L. 2004. Stress transfer at the interface of bonded joints between FRP and calcarenite natural stone. In Modena, Laurenço & Roca (eds), *IV Int. Seminar of Struct. Analysis of Hist. Constr.* Padua, 10-13 Nov.: 867-874.

ACI Committee 440. Guidelines for the design and construction of externally bonded FRP system for strengthening concrete structures. American Concrete Institute, Detroit, 2000.

Aiello, M.A., Sciolti, M.S. 2004. Analysis of bond performance between CFRP sheets and calcarenite ashlar under service and ultimate condition. In La Tegola & Nanni (eds), *Proc. of the 1st Int. Conf. on Innovative Materials and Techn. for Constr. and Restoration* Vol. 2: 81-96. Lecce, 6-9 June.

Arces, M., Nocilla, N., Aversa, S., Lo Cicero, G. 1998. Geological and geotechnical features of the "Calcarene di Marsala". In *Proc. of the 2nd Int. Symposium on Hard Soils – soft Rocks*: Naples, Italy 12-14 October.

Bizindavyi, L., Neale, K.W. 1997. Experimental and theoretical investigation of transfer lengths for composite laminates bonded to concrete. In *Proc., Annual Con. of Canadian Society for Civil Engng* Vol. 6: 51-60 Structures-Composites Materials, Structural Systems, Telecommunications Towers, Sherbrooke, Québec, Canada.

Bizindavyi, L., Neale, K.W. 1999. Transfer lengths and bond strengths for composites bonded to concrete. In *J. of Composite for Constr.*, ASCE, 3(4): 153-160.

Chajes, M.J., Finch, W. W., Januszka, T.F., Thonson, T. A. Jr. 1996. Bond and force transfer of composite material plates bonded to concrete. In *ACI Struct. J.*, 93 (2): 208-217.

Chen, J. F., Teng, J. G. 2001. Anchorage strength models for FRP and steel plates bonded to concrete. In *J. of Struct. Engng* ASCE, 127(7): 784-791.

CNR-DT200/2004. Istruzioni per la progettazione, l'esecuzione ed il controllo di interventi di consolidamento statico mediante l'utilizzo di compositi fibrorinforzati, Roma.

Cosenza, E., Manfredi, G., Occhiuzzi, A., Pecce, M. R. 2000. Toward the investigation of the interface behaviour between tuff masonry and FRP fabrics. In *Mechanics of Masonry Structures Strengthened with FRP Materials: Testing, Design, Control*: 99-108. 7-8 December, Venice.

De Lorenzis, L., Miller, B., Nanni, A. 2001. Bond of FRP Laminates to Concrete. In *ACI Materials J.*, 98 (3): 256-264.

Failla, A., Accardi, M., Rizzo, G., Algozzini, G., Pellitteri, G., Buscaglia, C., (2002). The use of CFRPs in strengthening of historical masonry structures: investigation on durability by accelerated testing. In Benmokrane & El-Salakawy (eds), *2nd Int. Conf. on Durability of fiber reinforced polymer (FRP) composites for construction*, Montreal 29-31 may, 297-303.

fib Bulletin, "Design and use of externally bonded FRP reinforcement for reinforced concrete structures", Bulletin no. 14, 2001, sub-group EBR of fib Task Group 9.3.

Holzenkämpfer, P. 1994. Ingenieurmodelle des verbundes geklebter bewehrung für betonbauteile. In *PhD dissertation*, TU Braunschweig, (in German).

JSCE Concrete Committee. 2001. Recommendations for upgrading of concrete structures with use of CFRP sheet.

Leung, C. K. Y. 2004. Fracture Mechanics of Debonding Failure. In *FRP-Strengthened Concrete Beams. FraMCoS-5*. April. Vail Cascade Resort, Vail, Colorado: 12-16.

Nakaba, K., Kanakubo, T., Furuta, T. Yoshizawa, H. 2001. Bond Behavior between Fiber-Reinforced Polymer Laminates and Concrete. In *ACI Struct. J.*, 98 (3): 359-367.

Neubauer, U. and Rostasy, F. S. 1997. Design aspects of concrete structures strengthened with externally bonded FRP plates. In *Proc., 7th Int. Conf. on Struct. Faults and Repair*, ECS Publications, Edinburgh, Scotland, 2: 109-118.

Qiu, Y., Crisfield, M. A., Alfano G. 2001. An interface element formulation for the simulation of delamination with buckling. In *Engineering fracture mechanics* 68: 1755-1776.

Savoia, M., Ferracuti, B. and Mazzotti, C. 2003. Non linear bond-slip law for FRP-concrete interface. In *FRPRCS-6:1-10*. Singapore.

Smith, S.T., Teng, J.G. 2002. FRP-strengthened RC beams. I: review of debonding strength models. In *Engng Struct.* 24: 385-395.

Täljsten, B. 1996. Strengthening of concrete prisms using the plate-bonding technique. In *Int. J. of Fract.* 82(3): 253-266.

Täljsten, B. 1997. Defining anchor lengths of steel and CFRP plates bonded to concrete. In *Int. Journal Adhesion and Adhesives*, 17(4): 319-327.

Wu, Z., Yuan, H., Niu, H. 2002. Stress transfer and fracture propagation in different kinds of adhesive joints. In *Journal of Engineering Mechanics*, ASCE 128 (5): 562-573.

Yuan, H. and Wu, Z. 1999. Interfacial fracture theory in structures strengthened with composite of continuous fiber. In *Proc., Symp. of China and Japan: Sci. and Technol. of 21st Century*, Tokyo, Sept., 142-155.

Yuan, H., Wu, Z., Yoshizawa, H. 2000. Theoretical solutions on interfacial stress transfer of externally bonded steel/composite laminates. In *J. Struct. Mechanics Earthquake Engng.*, 18(1): 27-39. Tokyo.